Oncogenic NRAS signaling differentially regulates survival and proliferation in melanoma

Lawrence N Kwong[1,2], James C Costello[3], Huiyun Liu[1], Shan Jiang[1,2], Timothy L Helms[2], Aliete E Langsdorf[1], David Jakubosky[1], Giannicola Genovese[1,2], Florian L Muller[1,2], Joseph H Jeong[1], Ryan P Bender[1], Gerald C Chu[1,4], Keith T Flaherty[5], Jennifer A Wargo[6], James J Collins[3,7] & Lynda Chin[1,2,8]

The discovery of potent inhibitors of the BRAF proto-oncogene has revolutionized therapy for melanoma harboring mutations in *BRAF*, yet *NRAS*-mutant melanoma remains without an effective therapy. Because direct pharmacological inhibition of the RAS proto-oncogene has thus far been unsuccessful, we explored systems biology approaches to identify synergistic drug combination(s) that can mimic RAS inhibition. Here, leveraging an inducible mouse model of *NRAS*-mutant melanoma, we show that pharmacological inhibition of mitogen-activated protein kinase kinase (MEK) activates apoptosis but not cell-cycle arrest, which is in contrast to complete genetic neuroblastoma RAS homolog (NRAS) extinction, which triggers both of these effects. Network modeling pinpointed cyclin-dependent kinase 4 (CDK4) as a key driver of this differential phenotype. Accordingly, combined pharmacological inhibition of MEK and CDK4 *in vivo* led to substantial synergy in therapeutic efficacy. We suggest a gradient model of oncogenic NRAS signaling in which the output is gated, resulting in the decoupling of discrete downstream biological phenotypes as a result of incomplete inhibition. Such a gated signaling model offers a new framework to identify nonobvious coextinction target(s) for combined pharmacological inhibition in *NRAS*-mutant melanomas.

The RAS proto-oncogene is activated across a diverse range of human cancers[1], including 15–20% of the melanomas that harbor activating *NRAS* mutations[2]. Agents that block canonical mitogen-activated protein kinase (MAPK) signaling components downstream of RAS, including the serine/threonine protein kinases BRAF, MEK and extracellular-signal–related kinase (ERK), have matured rapidly, with notably positive preclinical and clinical effects in several cancer types, particularly *BRAF*-mutant melanoma[3–7]. Clinically, single-agent MEK inhibition has limited efficacy against *NRAS*-mutant melanoma[7–9], and BRAF inhibitors have not been shown to be beneficial in *RAS*-mutant cancers[10–13]. Efforts to target oncogenic RAS mutants directly have thus far been unsuccessful.

Traditionally, RAS pathway diagrams depict a linear canonical MAPK cascade consisting of RAS, RAF, MEK and ERK, as well as other signaling branches emanating from RAS, such as the AKT proto-oncogene pathway. This signaling model has guided combination strategies to target RAS, such as co-inhibition of canonical MAPK (for example, MEK) and AKT signaling[14] or combined MEK and BRAF inhibition, to maximize the inhibition of MAPK signaling[15]. Despite these conceptual advances, key issues remain, including to what extent RAS-MAPK signaling can be maximally inhibited given the redundancy of its signaling network and whether there exist noncanonical coextinction strategies to approximate RAS inhibition.

The keys to data-driven discovery of new therapeutic combinations include not only robust computational platforms but also suitable and maneuverable experimental systems. Computational modeling of signaling pathways within individual cells has included a range of logic-based[16] and probabilistic models[17–19]. However, modeling the kinetics of such a network on an organismal level requires not only appropriate *in vivo* physiological systems but also the ability to easily perturb such systems for data acquisition. Inducible conditional genetically engineered mouse (GEM) models offer physiological systems that can be used to acquire global transcriptome and proteome data under various perturbation conditions (for example, genetic inactivation compared to pharmacological inhibition of an oncogene) over time. Notably, GEM models provide discrete and specific phenotypic correlates at both the organismal (for example, tumor growth and regression) and molecular (for example, apoptosis and cell-cycle arrest) levels *in vivo*. Integrating these input and output data would give a system-level view of a particular state after genetic or pharmacological inhibition to define nonobvious combination strategies.

In this study, we used this type of systems biology approach to discover evidence-based coextinction strategies against *NRAS*-mutant melanoma. In an inducible GEM model of melanoma driven by *NRAS* harboring a Q61K mutation (*NRAS*[Q61K]), we interrogated the network of oncogenic NRAS signaling using both genetic and pharmacological

perturbations. We show evidence for a model in which the signaling output downstream of NRAS-MEK-ERK is gated, resulting in the decoupling of two major cancer biological phenotypes, proliferation and survival, which in turn provides the molecular basis for coextinction of MEK and CDK4 to approximate NRAS inhibition.

RESULTS

NRAS[Q61K] extinction, but not MEK inhibition, regresses tumors

In the 'iNRAS' (inducible NRAS) GEM model of melanoma, expression of the melanoma signature mutation, *NRAS*[Q61K] (or oncogenic *NRAS*), is controlled by a doxycycline-regulated tet promoter on the background of a *Cdkn2a*-null allele; *CDKN2A* is a key human melanoma suppressor[20]. Doxycycline-inducible expression of *NRAS*[Q61K] is restricted to melanocytes through use of the Tyr-rtTA transgene[20]. Specifically, *NRAS*[Q61K] expression is driven by a Tet promoter that is activated only in the presence of both doxycycline and rtTA, with rtTA expression limited to melanocytes by the Tyr (tyrosinase) promoter. Administration of doxycycline to iNRAS mice at weaning thus turns on expression of the *NRAS*[Q61K] transgene in melanocytes and results in spontaneous melanoma formation with a 50% penetrance an average of 15 weeks after the start of treatment, whereas no melanomas develop in mice without doxycycline induction (**Supplementary Fig. 1a**).

In established tumors of both primary *de novo* and allograft transplant models (see Online Methods for derivation of iNRAS cell lines 413 and 475), doxycycline withdrawal turns off the tet-responsive promoter that drives expression of *NRAS*[Q61K]. At 4 d after doxycycline withdrawal, we found complete extinction of

NRAS[Q61K] transgene expression (**Fig. 1a**). Western blotting at the same time point (**Fig. 1b**) confirmed a loss of phosphorylated ERK (pERK). Phenotypically, loss of *NRAS*[Q61K] expression in the established melanomas resulted in rapid, durable and complete tumor regression within 10 d of doxycycline withdrawal (**Fig. 1c** and **Supplementary Fig. 1b,c**), validating *NRAS*[Q61K] as a tumor-maintenance oncogene. Of note, doxycycline withdrawal did not affect cell growth *in vitro* (**Supplementary Fig. 1d**), which is consistent with previous findings in a similarly engineered iHRAS model of melanoma[3], suggesting microenvironmental influences on tumor maintenance *in vivo*.

In the same *in vivo* allograft model system as described above, we treated mice bearing iNRAS melanomas with two different pharmacological MEK inhibitors (MEKi), specifically, the second-generation MEK inhibitor selumetinib (also known as AZD6244 or ARRY-142886)[21] or the third-generation MEK inhibitor GSK1120212 (also known as JTP-74057 or trametinib)[4]. Similar to other studies with human *NRAS*-mutant melanomas or xenografts[8,22], we found that MEKi was unable to induce tumor regression despite evidence that canonical MAPK signaling was inhibited, as determined by the amount of pERK present (**Fig. 1b**). Specifically, treatment with either single compound at its respective maximally tolerated dose resulted in tumor stasis but not tumor regression, in contrast to genetic extinction of *NRAS*[Q61K], which did result in tumor regression (**Fig. 1d**). This suggests that treatment with MEKi only partially inhibited oncogenic NRAS activity in the GEM model. Elucidation of the activity or activities unaffected by MEKi could lead to new target(s) for coextinction with MEKi.
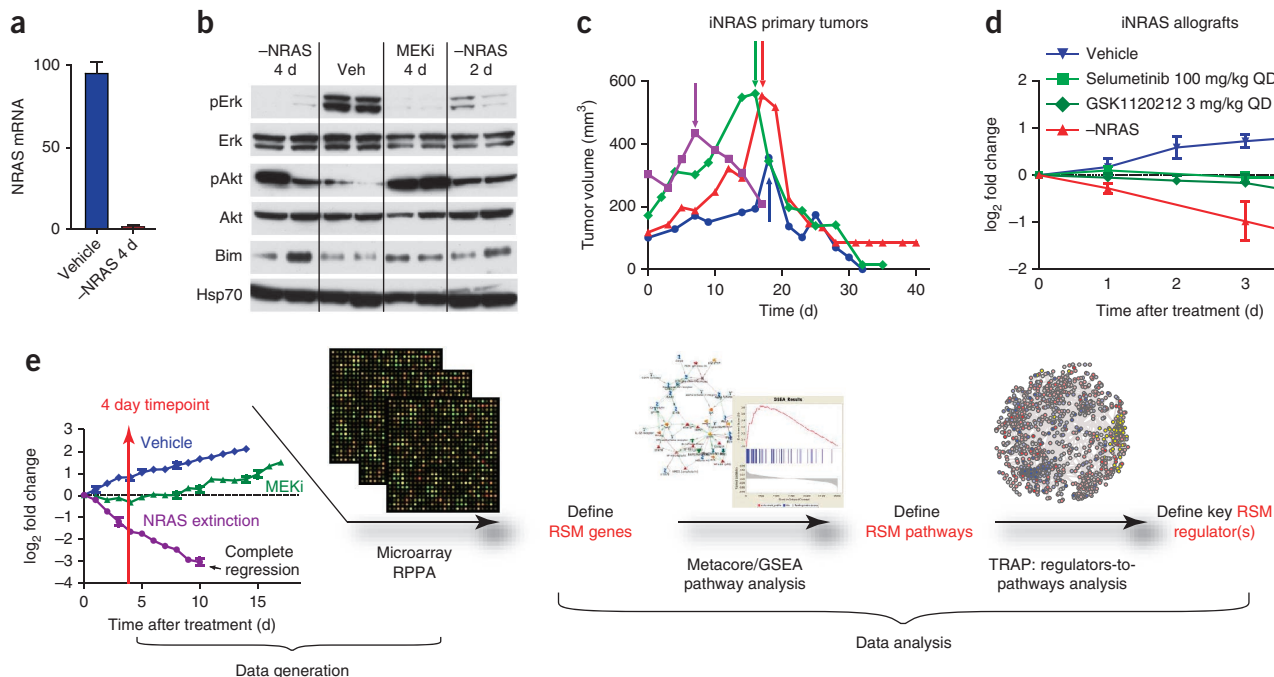

Figure 1 Characterization of the iNRAS mouse melanoma model and experimental design. (**a**) Transgene mRNA levels after 4 d of doxycycline withdrawal in iNRAS melanomas as determined by RT-PCR. –NRAS indicates doxycycline withdrawal for the number of days indicated. Data are means ± s.e.m. $n = 5$ tumors per cohort. (**b**) Western blot of pAkt, Akt, pErk, Erk and Bim from iNRAS cell line 413. Heat shock protein 70 (Hsp70) was used as a loading control. Veh, vehicle. (**c**) Tumor volumes from four independent iNRAS primary tumors (from one male and three female mice). Arrows indicate the start of doxycycline withdrawal. Different colors are shown for clarity to identify individual mice. (**d**) The effect of two different MEK inhibitors and doxycycline withdrawal on allograft tumor growth from iNRAS cell line 475 ($n = 6$ tumors per cohort). QD, daily. Data are means ± s.e.m. (**e**) Flow chart of the experimental design. Transcriptome data comparing genetic NRAS[Q61K] extinction and pharmacological MEK inhibition is processed through statistical and network analyses to generate RSM genes, pathways and, ultimately, pathway regulators. The tumor growth chart is taken from **Figure 5a**.
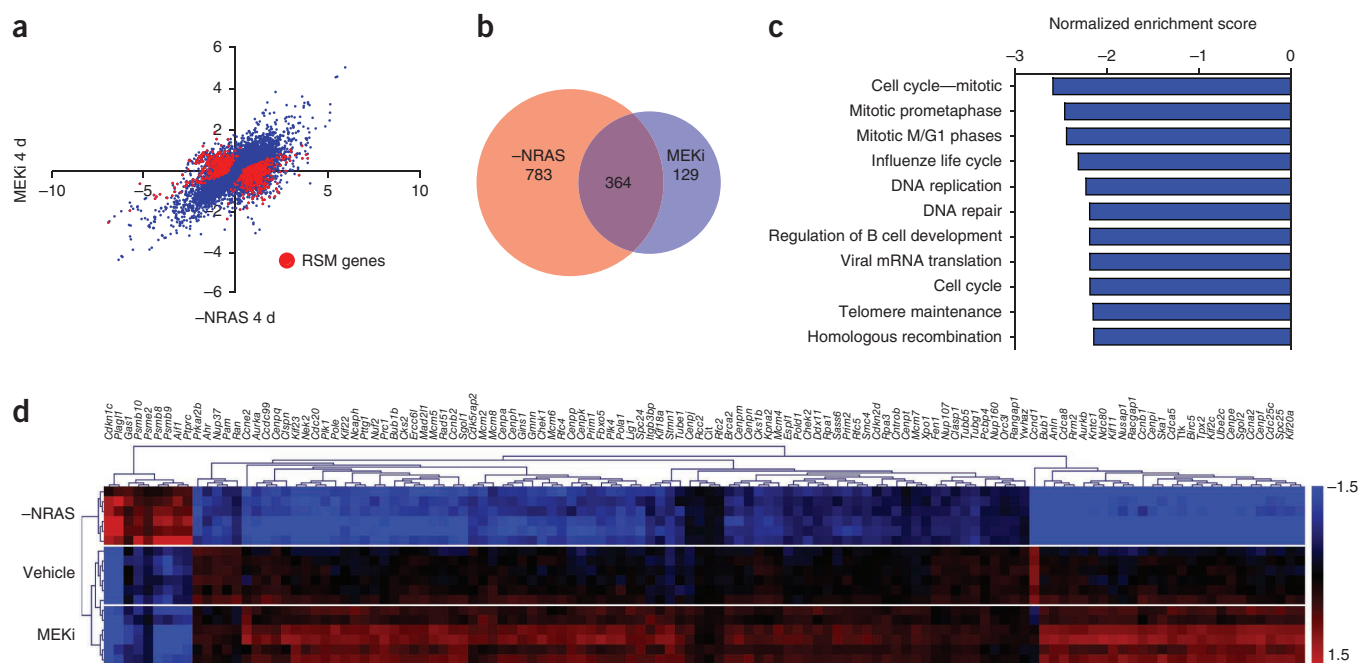
Figure 2 RAS-specific module (RSM) genes are highly enriched for cell-cycle functions. (**a**) Microarray data. The plot shows $\log_2$ fold change values of doxycycline withdrawal (–NRAS) and selumetinib treatment (MEKi) after 4 d compared to vehicle treatment in iNRAS cell line 475 allografts. Each point represents an average value ($n = 6$ tumors per cohort). RSM genes with Fisher combined $P < 10^{-5}$ are plotted in red, whereas non-RSM genes ($P > 10^{-5}$) are shown in blue. (**b**) Venn diagram showing the overlap in the number of differentially expressed genes shared by both MEKi and NRAS^{Q61K} extinction. (**c**) The top ten RSM pathways defined by GSEA analysis. Results from the Metacore analyses are shown in **Supplementary Table 4**. (**d**) Microarray heatmap of RSM genes from significant GSEA cell-cycle pathways with unsupervised hierarchical clustering.

Molecular phenotypes of *NRAS*^{Q61K} extinction versus MEKi

Using genetic extinction of *NRAS*^{Q61K} as the 'ground truth' representing complete RAS inhibition and pharmacological perturbation by MEKi as the comparator, we reasoned that global transcriptomic profiles and network modeling could uncover, in an unbiased manner, pathways or activities downstream of oncogenic NRAS that are not affected by treatment with MEKi. These pathways or activities would represent candidate coextinction targets that, in combination with MEKi, could approximate NRAS inhibition (**Fig. 1e**).

To this end, we compiled the transcriptomic profiles of iNRAS tumors after the two perturbations, genetic extinction of *NRAS*^{Q61K} and pharmacological inhibition by MEKi. Specifically, we harvested iNRAS allograft melanomas derived from a mouse melanoma

cell line, iNRAS-475, at 4 d after: doxycycline withdrawal, pharmacological MEK inhibition (daily maximal tolerated doses of selumetinib), or vehicle treatment ($n = 6$ per group) for transcriptome profiling (**Fig. 2a**). Using the criteria of a twofold change in expression and a q value $<10^{-3}$, we found that 74% (364/493) of the genes that were
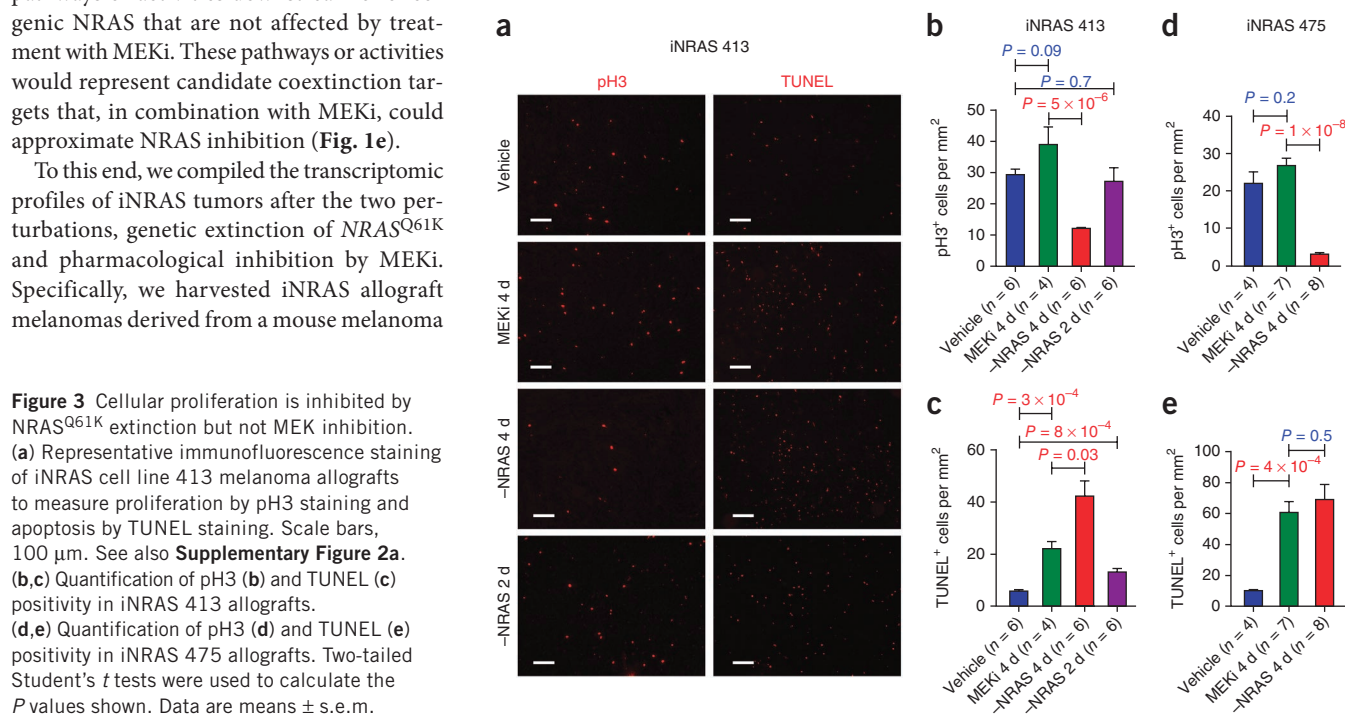
Figure 3 Cellular proliferation is inhibited by NRAS^{Q61K} extinction but not MEK inhibition. (**a**) Representative immunofluorescence staining of iNRAS cell line 413 melanoma allografts to measure proliferation by pH3 staining and apoptosis by TUNEL staining. Scale bars, 100 μm. See also **Supplementary Figure 2a**. (**b,c**) Quantification of pH3 (**b**) and TUNEL (**c**) positivity in iNRAS 413 allografts. (**d,e**) Quantification of pH3 (**d**) and TUNEL (**e**) positivity in iNRAS 475 allografts. Two-tailed Student's *t* tests were used to calculate the *P* values shown. Data are means ± s.e.m.

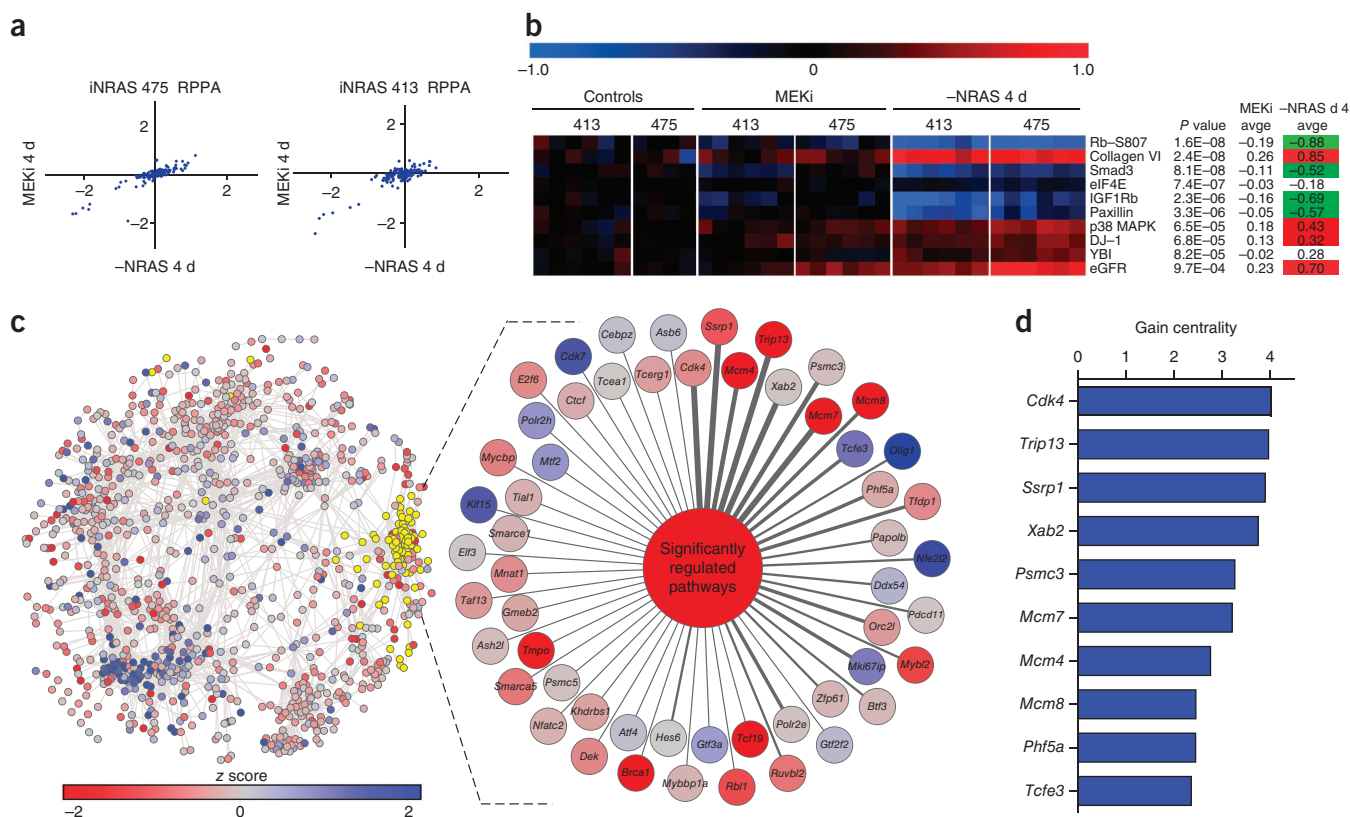**Figure 4** The Cdk4-Rb axis regulates the RAS-specific pathways. (**a**) Reverse-phase protein array data. The plot shows $\log_2$ fold change values of doxycycline withdrawal (–NRAS) compared to selumetinib treatment (MEKi) after 4 d compared to vehicle in two independent iNRAS allograft cohorts, cell lines 413 and 475. Each point represents an average value ($n = 6$ tumors cohort, except $n = 4$ tumors for the iNRAS 475 vehicle-treated group). (**b**) RPPA heatmap of the top ten RSM proteins, including the RSM P values (Fisher combined P values, see Online Methods) and averages (avge). Vehicle represents the control. (**c**) TRAP network overlaid with microarray and GSEA data and colored according to z score. The yellow highlighted nodes represent the 41 significantly downregulated pathways identified through GSEA and the 55 first-neighbor regulator genes. The enlargement shows all 55 regulators connected to a generic node representing the downregulated pathways. See **Supplementary Table 3** for a list of all pathways. The regulators have been ordered clockwise based on the number of edges they share with the pathways, which is reflected in the edge thickness. (**d**) Top ten pathway regulators ranked by gain in degree centrality, which is a measurement of regulator strength that takes into account both weighted edge strength and the normalized connectivity of the regulators in the subnetwork of RSM pathways compared to all pathways. See **Supplementary Table 7** for the full ranked list of 55 regulators.

differentially regulated by selumetinib were also similarly modulated by $NRAS^{Q61K}$ extinction (**Fig. 2b**). This set of 364 overlapping genes was enriched for canonical downstream ERK targets and pathway sensors such as *Maff*, *Fosl1*, *Spry4*, *Dusp4* and *Etv4* (ref. 23) (**Supplementary Table 1**), corroborating the western blot data showing that canonical MAPK signaling was inhibited in both settings (**Fig. 1b**).

Next, to delineate the activity that was affected by $NRAS^{Q61K}$ extinction but not MEK inhibition, we defined a RAS-specific module (RSM) comprising genes whose expressions showed statistically significant regulation by $NRAS^{Q61K}$ extinction but showed either no change or a change in the opposite direction as a result of selumetinib treatment (Fisher combined $P < 1 \times 10^{-5}$; **Fig. 2a** and **Supplementary Table 2**). Knowledge-based pathway analyses by gene set enrichment analysis (GSEA)[24] using an RSM-ranked list of genes (Online Methods) and Metacore revealed a dominance of pathways directly related to cell-cycle regulation enriched among the RSM genes (**Fig. 2c,d** and **Supplementary Tables 3** and **4**). No other canonical oncogenic signaling pathway, including phosphatidylinositol-4,5-bisphosphate 3-kinase (Pi3k), transforming growth factor β (Tgf-β), Wnt, or c-Jun N-terminal kinase (Jnk) signaling (**Supplementary Tables 3** and **4**), showed statistically significant enrichment ($P > 0.05$).

The knowledge-based pathway analysis described above suggested that a major explanation for the inability of pharmacological MEK inhibition to induce tumor regression is its inability to engage the cell-cycle checkpoint in iNRAS melanomas. This finding seems counterintuitive given that RAS-MEK-ERK signaling has been intimately linked to cell proliferation[25]. Thus, we sought to confirm this analytical result by quantifying mitosis and apoptosis in histological sections of tumors derived from two independent iNRAS melanoma cell lines, iNRAS-413 and iNRAS-475 (**Fig. 3**). Staining for phosphorylated histone H3 (pH3) revealed a statistically significant inhibition of mitotic activity after genetic extinction of $NRAS^{Q61K}$ in both cohorts (**Fig. 3a,b,d** and **Supplementary Fig. 2a**). Consistent with the pathway analysis results, we found no statistically significant changes in mitotic activity, as determined by pH3 staining (**Fig. 3a,b,d** and **Supplementary Fig. 2**) or BrdU incorporation (**Supplementary Fig. 2b**), in tumors treated with the maximally tolerated doses of either selumetinib or GSK1120212 after 4 d of daily dosing. In contrast, TUNEL staining for apoptotic cells revealed a statistically significant induction of apoptosis by both genetic $NRAS^{Q61K}$ extinction and pharmacological MEK inhibition (**Fig. 3a,c,e** and **Supplementary Fig. 2a**). Correspondingly, Bim and Bmf, which are central to the induction of apoptosis after MAPK pathway inhibition[26], were upregulated to similar extents by $NRAS^{Q61K}$ extinction and

Figure 5 The combination MEK and CDK4/6 inhibition is synergistic *in vivo*. (**a**) Mouse cell line iNRAS 475 allografts treated with PD-0332991 (PD) and GSK1120212 (GSK) singly or in combination. Doxycycline withdrawal (–NRAS) is shown for comparison. QD, daily; QOD, every other day; CR, complete response. All data in this figure are means ± s.e.m. (**b**) Human NRAS[Q61K] cell line SB-2 xenografts treated with PD-0332991 and GSK1120212 singly or in combination. (**c**,**d**) Quantification of pH3 (**c**) and TUNEL (**d**) positivity in SB-2 tumors after 4 d of treatment. Two-tailed Student's *t* tests were used to calculate the *P* values shown. (**e**) Representative BrdU and cleaved caspase-3 (Casp3) immunohistochemistry from treated EVOC tumor slices after 3 d of treatment. (**f**,**g**) Quantification of BrdU (**f**) and caspase-3 (**g**) positivity in EVOC tumor slices. Scale bars, 200 μm.

selumetinib treatment at both the mRNA and the protein level (**Fig. 1b** and **Supplementary Fig. 3**). Taken together, the experimental data and computational analyses collectively show that pharmacological MEK inhibition efficiently induces apoptosis but not cell-cycle arrest, which is in contrast to the dual effect of NRAS[Q61K] genetic extinction.

We further reinforced this conclusion using a targeted proteome analysis by reverse phase protein array (RPPA) profiling of 120 signaling proteins and phospho-specific states. Similar to the microarray data, the genetic and pharmacological perturbations showed a high degree of overlap in global protein changes (**Fig. 4a**). However, consistent with the gene expression analysis results, the most significantly differentially modulated RAS-specific protein across the two independent cohorts assayed above was the phosphorylated and, thus, inactivated form of the tumor suppressor retinoblastoma protein (Rb) (**Fig. 4b**). Specifically, tumors subjected to NRAS[Q61K] extinction harbored statistically significantly lower amounts of phosphorylated Rb compared to tumors treated with MEK inhibitor or vehicle (**Fig. 4b** and **Supplementary Fig. 4**), suggesting that the Rb checkpoint is differentially activated by these two perturbations.

Network modeling pinpoints Cdk4 as a MEK coextinction target
To identify the principal driver of the molecular differences between the genetic and pharmacological perturbations, we used a new network inference algorithm, transcriptional regulatory associations in pathways (TRAP). In contrast to a gene-gene network, TRAP was designed to identify gene-pathway transcriptional regulatory relationships, where the gene is a transcriptional regulator and the pathway is an annotated biological pathway or process (**Supplementary Fig. 5** and **Online Methods**). Briefly, we constructed a global regulator-pathway network for mouse based on a compendium of over 3,000 public microarray profiles spanning a wide range of experimental conditions and perturbations (but not including the profiles of the iNRAS melanomas used in this study). For each pathway defined by the Molecular Signatures Database (MSigDB) v3 (ref. 27), we calculated a pathway's activity as the average expression of its constituent genes (not including the transcription regulators themselves). Next, we computed mutual information for all regulator-pathway pairs, we applied a background correction to account for indirect regulation and, finally, calculated a statistic on each regulator-pathway pair. The resultant TRAP network

(**Fig. 4c**) therefore captures the most significant regulator-pathway associations within the large compendium of expression profiles.

Using the TRAP network, we investigated which regulators are most significantly linked to (that is, are candidate drivers of) the key pathway differences between genetic and pharmacological perturbations in the iNRAS model. We selected the first neighbor regulators connected to each of the highest-ranking 41 pathways enriched in the RAS-specific module by GSEA (false discovery rate <10[−3]). We next ranked the regulators on the basis of degree centrality, which is a measure of the number and strength of the connections to these pathways. In this manner, TRAP ranked 55 candidate regulators that were connected to pathways enriched in the RSM genes (**Fig. 4c,d** and **Supplementary Tables 5**–**7**). Consistent with the experimental data showing cell-cycle arrest as a key phenotypic difference between the genetic and pharmacological perturbations, the regulator ranked highest by TRAP was Cdk4, a well-known proximal regulator of the Rb-regulated G1/S cell-cycle checkpoint. Western blotting confirmed that Cdk4 was affected by complete NRAS[Q61K] extinction but not MEKi treatment (**Supplementary Fig. 4**). Notably, the related cell-cycle agonists Cdk2 (which also phosphorylates Rb), Cdk7 and Cdk9 were not ranked as being significant by TRAP.

In summary, global network modeling by TRAP not only confirmed the Rb-regulated cell-cycle checkpoint as a target that is differentially affected by genetic NRAS[Q61K] extinction compared to pharmacological MEK inhibition but also pinpointed Cdk4 as a key driver of the molecular differences correlating with the different phenotypic consequences, namely, tumor regression compared to tumor stasis.

Combined MEK and CDK4/6 inhibition is synergistic *in vivo*
The unbiased network modeling analysis suggested Cdk4 as a coextinction target with MEK. Because a selective dual inhibitor of CDK4 and CDK6 (hereafter referred to as CDK4/6), PD-0332991, is currently under clinical development, we sought to experimentally
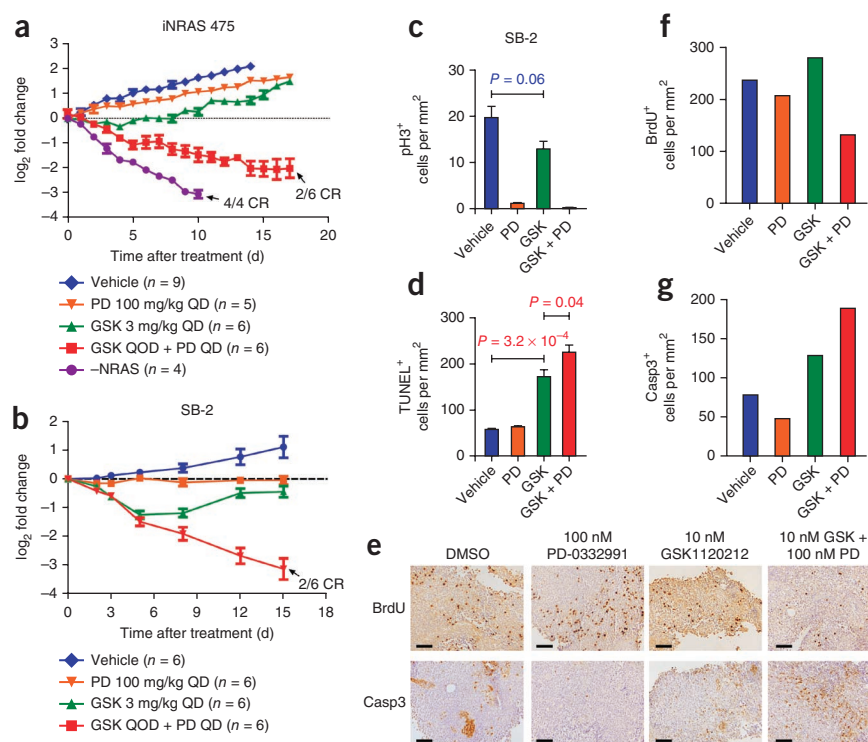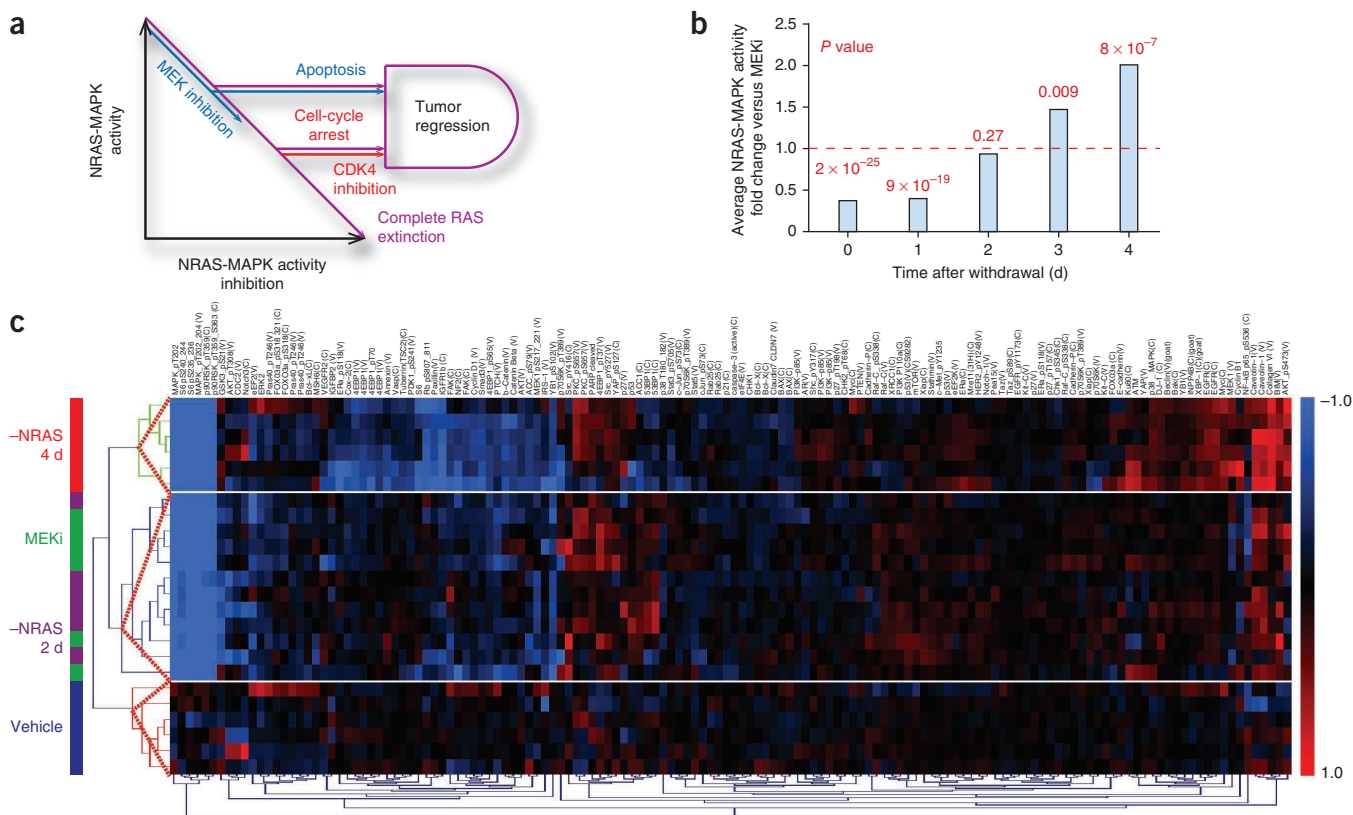
Figure 6 NRAS-MAPK activity differentially regulates apoptosis and proliferation. (**a**) A model of oncogenic NRAS signaling as a gradient with gated phenotypic outputs. As NRAS-MAPK activity is inhibited, apoptosis and cell-cycle arrest are triggered at different amounts of activity. Complete RAS extinction (purple) or combined inhibition of MEK (blue) and CDK4 (red) complementarily trigger both phenotypes, fulfilling the dual input into the AND gate required for efficient tumor regression. In logic, AND gates require simultaneous truth statements to produce an output. (**b**) Comparison of the average NRAS-MAPK activity in the gene set at various time points after doxycycline withdrawal compared to the activity resulting from MEKi treatment. *P* values for these comparisons are indicated above each bar. A paired Student's *t* test of the unlogged fold-change values was used to calculate the *P* values. (**c**) Unsupervised hierarchical clustering of RPPA data from iNRAS 413 tumors treated with vehicle, MEKi or 2 d or 4 d of doxycycline withdrawal.

validate this predicted synergy between inhibition of MEK and CDK4. Of note, PD-0332991 has been reported to inhibit cell proliferation *in vivo* without enhancing apoptosis[28], unlike other cell-cycle inhibitors targeting CDK1, CDK2, CDK9, aurora kinase (AURK) or polo-like kinase (PLK)[29,30], which do both. Indeed, *in vivo* administration of PD-0332991 and either selumetinib (**Supplementary Fig. 6a**) or GSK1120212 (**Fig. 5a**) induced potent synergy in iNRAS allograft tumors, resulting in not just tumor stasis but a clear regression, including two complete responses (no residual palpable tumor) in the cohort treated with GSK1120212 (**Fig. 5a** and **Supplementary Fig. 6b**). Notably, this efficacy was achieved at submaximal tolerated doses of each inhibitor.

Similarly, in two independent *NRAS*-mutant human melanoma cell lines, SB-2 and HMVII, combined treatment with PD-0332991 and GSK1120212 in xenograft tumors revealed a synergistic antioncological efficacy (**Fig. 5b** and **Supplementary Fig. 7a**). Specifically, MEK inhibition alone in these human melanoma xenografts induced apoptosis but not cell-cycle arrest (**Fig. 5c,d** and **Supplementary Fig. 7b,c**), establishing that this is not a mouse-specific phenomenon. Treatment with the CDK4/6 inhibitor alone suppressed cell proliferation but did not have any effect on apoptosis. The combination of PD-0332991 and GSK1120212 at submaximal doses resulted in both apoptosis and cell-cycle arrest in the xenograft tumors, with corresponding tumor regression,

including two complete responses in the SB-2 cohort (**Fig. 5b–d** and **Supplementary Fig. 7a–d**). Although we observed some weight loss with PD-0332991 treatment, as has been previously reported[28], this effect was not significantly exacerbated by MEK inhibition (**Supplementary Fig. 7e,f**), suggesting a lack of an adverse interaction between the two drugs. To further substantiate the human relevance of this observation, we tested a freshly biopsied human *NRAS*-mutant tumor in an *ex vivo* system called *ex vivo* organotype culture (EVOC) (Online Methods). MEKi treatment with measurable pERK inhibition (**Supplementary Fig. 8**) induced apoptosis but not cell-cycle arrest in this system, as measured by cleaved caspase-3 staining and BrdU incorporation, respectively (**Fig. 5e–g**). Only the combination of the two inhibitors enhanced both phenotypes (**Fig. 5e–g**). In summary, in both GEM and human melanoma model systems, combined treatment with pharmacological inhibitors of CDK4 and MEK was potently synergistic.

Gated *NRAS*^Q61K signaling decouples survival and proliferation

Although there was a substantial overlap in genes co-regulated by both MEKi and *NRAS*^Q61K extinction (**Fig. 2b**), especially among known canonical downstream ERK targets and pathway sensors (**Supplementary Table 1**), it was notable that genetic *NRAS*^Q61K extinction produced global gene expression and protein changes of larger amplitude than MEKi treatment (**Figs. 2a** and **4a**). To quantify

this effect, we defined a gene set comprising 49 MAPK-regulated genes that are conserved between mouse and human (**Supplementary Table 8** and Online Methods)[31–33] that was similar to gene sets previously reported in other studies[32,34]. We then used this gene set as a surrogate measure of oncogenic NRAS^{Q61K} activity propagating down the canonical MAPK signaling cascade (NRAS-MAPK activity). Applying a paired Student's t test to restrict the comparison to matched gene measurements while generating a signature-wide significance score, we found that, on average, genetic extinction of *NRAS*^{Q61K} was approximately twice as effective as MEKi treatment in suppressing NRAS-MAPK activity ($P = 7.8 \times 10^{-7}$; **Supplementary Table 8**). This difference in degree of inhibition raised the possibility that NRAS-MAPK activity is not a binary on/off signal but, rather, is an analog output over a gradient. If downstream phenotypes such as proliferation and survival have differential sensitivities to the amount of NRAS-MAPK activity, gated outputs would be generated (**Fig. 6a**). In other words, this model would predict that when NRAS-MAPK activity is only partially inhibited along the gradient (for example, by a pharmacological inhibitor of MEK), only apoptosis would be triggered if the residual MAPK signaling is sufficient to drive proliferation. Thus, complete (or near-complete) inhibition (for example, by genetic extinction) would be required to additionally induce cell-cycle arrest.

To test this hypothesis, we sought to create a state of partial genetic NRAS-MAPK inhibition similar to that achieved by pharmacological MEK inhibition. Specifically, we computed a measure of NRAS-MAPK activity using the MAPK-regulated gene set described above and transcriptome data of iNRAS melanomas after doxycycline withdrawal over a 4-d time course. We found that the degree of NRAS-MAPK inhibition at 2 d after doxycycline withdrawal was most similar to that achieved by MEKi treatment ($P = 0.27$; **Fig. 6b** and **Supplementary Table 8**). Reinforcing this finding, unsupervised hierarchical clustering of the RPPA profiles revealed coclustering of the group at 2 d after doxycycline withdrawal and the group treated with MEKi (**Fig. 6c**). Taking these results to suggest a partial inhibition state at 2 d after doxycycline withdrawal, we next quantified cell proliferation and apoptosis in this withdrawal group by immunohistopathology. We found that iNRAS melanomas at 2 d after doxycycline withdrawal showed no significant change in mitotic index ($P = 0.07$; **Fig. 3b**), pRb or Cdk4 protein concentrations (**Supplementary Figs. 4** and **9**) but did have elevated amounts of apoptosis (**Fig. 3c**) and Bim (**Fig. 1b**). In other words, partial genetic extinction of NRAS-MAPK activity resulted in the induction of apoptosis but not cell-cycle arrest, similar to the effect seen with MEKi treatment. Taken together, these data support the model that oncogenic NRAS signaling to the canonical MAPK cascade is not binary but, instead, is analog, producing a gradient of activity that triggers discrete biological phenotypes at different thresholds (**Fig. 6a**).

DISCUSSION

In this study, we exploited the experimental merits of the mouse and the advantages of the field of systems biology to understand the actions of activated RAS signaling in cancer. By comparing the molecular changes induced by genetic NRAS^{Q61K} extinction to those induced by pharmacological MEK inhibition using a knowledge-based pathway analysis and global network modeling, supported by histopathological validation of the tumors, we found that MEK inhibitors did not engage the cell-cycle checkpoint, resulting in tumor stasis but not regression despite robust apoptosis. Using an intermediate time point at which NRAS-MAPK activity was only partially extinguished by genetic means, we provided experimental support for a gated model of canonical NRAS-MAPK signaling that regulates its

two major downstream phenotypes at different thresholds (**Fig. 6a**). Such a gated output model explains the finding that treatment with MEKi induced apoptosis but not cell-cycle arrest in our iNRAS model, providing a rationale for combining a CDK4 inhibitor with MEKi to achieve therapeutic synergy. However, our data do not rule out alternative molecular mechanisms underlying this synergy. Of note, a recent study reported that Cdk4 is synthetic lethal in *Kras*-mutant mouse lung cancer cells[35]. Although the study did not suggest, either experimentally or mechanistically, that combined Cdk4 and Mek inhibition could be synergistic, this finding of synthetic lethality raises the possibility that this gated-output model of NRAS-MAPK signaling could be operative in mutant KRAS signaling despite differences in the functions of KRAS and NRAS[36].

Our experimental findings are of clinical relevance, as complete shutoff of oncogenic NRAS signaling to downstream RAF-MEK-ERK may be difficult to achieve pharmacologically given the redundant feedbacks and the probable induction of toxicity in patients[37]. The combined inhibition of two orthogonal targets may offer the advantage of a wider therapeutic window given the differing toxicity profiles of the two drugs[37,38]. More broadly, the gated signaling model provides a new framework for developing combination strategies for pathway inhibition, specifically, by complementing partial inhibition by one drug with another drug that targets a decoupled phenotype of the same signaling pathway. It is clear that simultaneous inhibition of CDK4 and MEK, although synergistic, does not fully recapitulate the complete tumor-regression phenotype achieved by genetic NRAS^{Q61K} extinction. Although this incomplete effect may be the result of imperfect target inhibition or pharmacokinetics, it is possible that additional oncogenic NRAS-dependent activity (or activities) may also need to be inhibited to more perfectly mimic direct RAS inhibition.

In conclusion, the convergence of advanced genomic technologies, maturing network modeling methodologies and sophisticated inducible GEM models of cancers that enable perturbation of key targets in a controlled manner provides a framework for the systematic design and execution of preclinical studies for an emerging pharmacological agent. The faithfulness of GEM models, the relative ease of access to tumor tissues before and after dosing, and the ability of the models to produce an otherwise unachievable ground truth frame of reference for the drug together make for an ideal system for the study and understanding of therapeutic responses and resistance, informing on a clinical path hypothesis. Systems-level approaches here enabled us to model the data in an unbiased and physiological setting to pinpoint NRAS^{Q61K}-activity–dependent differences in the key phenotypic outputs of survival and proliferation. Ultimately, such analyses arrived at an unanticipated yet efficacious strategy, inhibition of both MEK and CDK4, for targeting this intractable tumor type. This is a key complement to the knowledge-based approach of designing combination strategies based on existing pathway models.

METHODS

Methods and any associated references are available in the online version of the paper.

Note: Supplementary information is available in the online version of the paper.

AUTHOR CONTRIBUTIONS

L.N.K. performed the majority of experiments described in the manuscript. J.C.C. performed GSEA and TRAP analyses. L.N.K. and J.C.C. jointly generated the remaining statistics. H.L. and T.L.H. helped maintain nude mouse colonies and provided technical assistance in many experiments. S.J. maintained the iNRAS GEM model colony and measured tumor volumes for primary melanomas. A.E.L., D.J. and G.C.C. performed the EVOC work, and the biopsy was supplied by J.A.W. and K.T.F. G.G. and F.L.M. performed some western blotting. J.H.J. generated the iNRAS mouse. R.P.B. assisted in generating the iNRAS time course microarray data. J.J.C. oversaw TRAP and statistical analyses. L.N.K. and L.C. conceived of the study. L.N.K., J.C.C. and L.C. wrote the paper.

COMPETING FINANCIAL INTERESTS

1. Schubbert, S., Shannon, K. & Bollag, G. Hyperactive Ras in developmental disorders and cancer. *Nat. Rev. CancerNatl. Rev.* **7**, 295–308 (2007).
2. Jakob, J.A. *et al.* NRAS mutation status is an independent prognostic factor in metastatic melanoma. *Cancer* **118**, 4013–4023 (2011).
3. Flaherty, K.T. *et al.* Inhibition of mutated, activated BRAF in metastatic melanoma. *N. Engl. J. Med.* **363**, 809–819 (2010).
4. Gilmartin, A.G. *et al.* GSK1120212 (JTP-74057) is an inhibitor of MEK activity and activation with favorable pharmacokinetic properties for sustained *in vivo* pathway inhibition. *Clin. Cancer Res.* **17**, 989–1000 (2011).
5. Bollag, G. *et al.* Clinical efficacy of a RAF inhibitor needs broad target blockade in BRAF-mutant melanoma. *Nature* **467**, 596–599 (2010).
6. Flaherty, K.T. *et al.* Improved survival with MEK inhibition in BRAF-mutated melanoma. *New Engl. J. Med.* **367**, 107–114 (2012).
7. Falchook, G.S. *et al.* Activity of the oral MEK inhibitor trametinib in patients with advanced melanoma: a phase 1 dose-escalation trial. *Lancet Oncol.* **13**, 782–789 (2012).
8. Kirkwood, J.M. Phase II, open-label, randomized trial of the MEK1/2 inhibitor selumetinib as monotherapy versus temozolomide in patients with advanced melanoma. *Clin. Cancer Res.* **18**, 555–567 (2012).
9. Ascierto, P.A. *et al.* Efficacy and safety of oral MEK162 in patients with locally advanced and unresectable or metastatic cutaneous melanoma harboring BRAFV600 or NRAS mutations. *J. Clin. Oncol.* **30**, suppl; abstr 8511 (2012).
10. Hatzivassiliou, G. *et al.* RAF inhibitors prime wild-type RAF to activate the MAPK pathway and enhance growth. *Nature* **464**, 431–435 (2010).
11. Poulikakos, P.I., Zhang, C., Bollag, G., Shokat, K.M. & Rosen, N. RAF inhibitors transactivate RAF dimers and ERK signalling in cells with wild-type BRAF. *Nature* **464**, 427–430 (2010).
12. Heidorn, S.J. *et al.* Kinase-dead BRAF and oncogenic RAS cooperate to drive tumor progression through CRAF. *Cell* **140**, 209–221 (2010).
13. Su, F. *et al.* RAS mutations in cutaneous squamous-cell carcinomas in patients treated with BRAF inhibitors. *N. Engl. J. Med.* **366**, 207–215 (2012).
14. Villanueva, J. *et al.* Acquired resistance to BRAF inhibitors mediated by a RAF kinase switch in melanoma can be overcome by cotargeting MEK and IGF-1R/PI3K. *Cancer Cell* **18**, 683–695 (2010).
15. Paraiso, K.H. *et al.* Recovery of phospho-ERK activity allows melanoma cells to escape from BRAF inhibitor therapy. *Br. J. Cancer* **102**, 1724–1730 (2010).
16. Morris, M.K., Saez-Rodriguez, J., Sorger, P.K. & Lauffenburger, D.A. Logic-based models for the analysis of cell signaling networks. *Biochemistry* **49**, 3216–3224 (2010).
17. Sachs, K., Gifford, D., Jaakkola, T., Sorger, P. & Lauffenburger, D.A. Bayesian network approach to cell signaling pathway modeling. *Sci. STKE* **2002**, pe38 (2002).
18. Della Gatta, G. *et al.* Reverse engineering of TLX oncogenic transcriptional networks identifies RUNX1 as tumor suppressor in T-ALL. *Nat. Med* **18**, 436–440 (2012).
19. Belcastro, V. *et al.* Transcriptional gene network inference from a massive dataset elucidates transcriptome organization and gene function. *Nucleic Acids Res.* **39**, 8677–8688 (2011).
20. Chin, L. *et al.* Essential role for oncogenic Ras in tumour maintenance. *Nature* **400**, 468–472 (1999).
21. Yeh, T.C. *et al.* Biological characterization of ARRY-142886 (AZD6244), a potent, highly selective mitogen-activated protein kinase kinase 1/2 inhibitor. *Clin. Cancer Res.* **13**, 1576–1583 (2007).
22. Solit, D.B. *et al.* BRAF mutation predicts sensitivity to MEK inhibition. *Nature* **439**, 358–362 (2006).
23. Pratilas, C.A. *et al.* (V600E)BRAF is associated with disabled feedback inhibition of RAF-MEK signaling and elevated transcriptional output of the pathway. *Proc. Natl. Acad. Sci. USA* **106**, 4519–4524 (2009).
24. Subramanian, A. *et al.* Gene set enrichment analysis: a knowledge-based approach for interpreting genome-wide expression profiles. *Proc. Natl. Acad. Sci. USA* **102**, 15545–15550 (2005).
25. Luo, J. *et al.* A genome-wide RNAi screen identifies multiple synthetic lethal interactions with the Ras oncogene. *Cell* **137**, 835–848 (2009).
26. VanBrocklin, M.W., Verhaegen, M., Soengas, M.S. & Holmen, S.L. Mitogen-activated protein kinase inhibition induces translocation of Bmf to promote apoptosis in melanoma. *Cancer Res.* **69**, 1985–1994 (2009).
27. Liberzon, A. *et al.* Molecular signatures database (MSigDB) 3.0. *Bioinformatics* **27**, 1739–1740 (2011).
28. Fry, D.W. *et al.* Specific inhibition of cyclin-dependent kinase 4/6 by PD 0332991 and associated antitumor activity in human tumor xenografts. *Mol. Cancer Ther.* **3**, 1427–1438 (2004).
29. Shapiro, G.I. Cyclin-dependent kinase pathways as targets for cancer treatment. *J. Clin. Oncol.* **24**, 1770–1783 (2006).
30. Lens, S.M., Voest, E.E. & Medema, R.H. Shared and separate functions of polo-like kinases and aurora kinases in cancer. *Nat. Rev. CancerNatl. Rev.* **10**, 825–841 (2010).
31. Joseph, E.W. *et al.* The RAF inhibitor PLX4032 inhibits ERK signaling and tumor cell proliferation in a V600E BRAF-selective manner. *Proc. Natl. Acad. Sci. USA* **107**, 14903–14908 (2010).
32. Packer, L.M., East, P., Reis-Filho, J.S. & Marais, R. Identification of direct transcriptional targets of (V600E)BRAF/MEK signalling in melanoma. *Pigment Cell Melanoma Res.* **22**, 785–798 (2009).
33. Hoeflich, K.P. *et al.* Antitumor efficacy of the novel RAF inhibitor GDC-0879 is predicted by BRAFV600E mutational status and sustained extracellular signal-regulated kinase/mitogen-activated protein kinase pathway suppression. *Cancer Res.* **69**, 3042–3051 (2009).
34. Dry, J.R. *et al.* Transcriptional pathway signatures predict MEK addiction and response to selumetinib (AZD6244). *Cancer Res.* **70**, 2264–2273 (2010).
35. Puyol, M. *et al.* A synthetic lethal interaction between K-Ras oncogenes and Cdk4 unveils a therapeutic strategy for non-small cell lung carcinoma. *Cancer Cell* **18**, 63–73 (2010).
36. Haigis, K.M. *et al.* Differential effects of oncogenic K-Ras and N-Ras on proliferation, differentiation and tumor progression in the colon. *Nat. Genet.* **40**, 600–608 (2008).
37. Adjei, A.A. *et al.* Phase I pharmacokinetic and pharmacodynamic study of the oral, small-molecule mitogen-activated protein kinase kinase 1/2 inhibitor AZD6244 (ARRY-142886) in patients with advanced cancers. *J. Clin. Oncol.* **26**, 2139–2146 (2008).
38. Schwartz, G.K. *et al.* Phase I study of PD 0332991, a cyclin-dependent kinase inhibitor, administered in 3-week cycles (Schedule 2/1). *Br. J. Cancer* **104**, 1862–1868 (2011).

ONLINE METHODS

RNA extraction and expression microarrays. We homogenized tumors in TRIzol solution. We extracted nucleic acids using phenol and chloroform, precipitated them with isopropanol, washed them with 70% ethanol and resuspended them in RNAse-free water. DNA was removed using DNAse in the presence of RNAse inhibitors (Promega) by incubating for 40 min at 37 °C. Samples were processed through the RNEasy kit (Qiagen) to wash and elute the RNA. Samples were tested for purity by measuring 260/230 and 260/280 values on a Nanodrop machine (Thermo Scientific). These absorption ratios measure the purity of nucleic acids by spectrophotometry. Impure samples (<1.8 ratio) were repurified using standard ethanol precipitation. Further quality control was performed by the Dana-Farber Cancer Institute Microarray Core facility (http://chip.dfci.harvard.edu/) using the Bioanalyzer platform (Agilent). A minimum of 1 µg of RNA per sample was run on a Mouse Genome 430 2.0 Array (Affymetrix). Microarray data are accessible through GEO (Gene Expression Omnibus) under the accession numbers GSE39984 and GSE39985.

Real-time PCR. We ran real-time PCR on an MX3000P machine (Agilent) using Express SYBR-GreenER (Invitrogen). Expression of the human NRAS[Q61K] transgene was detected using the following primers: forward, 5′-GGATACCAGCTGGAaAAGAAGAG-3′; reverse, 5′-TTCCCACTACGACCATAGGTAC-3′. The lowercase a denotes the Q61K mutation. Results were normalized to glyceraldehyde 3-phosphate dehydrogenase (GAPDH).

Western blotting and reverse-phase protein arrays. We homogenized tumors to extract protein in radioimmunoprecipitation assay (RIPA) buffer plus phosphatase and protease inhibitors (Sigma) and sonicated them to shear genomic DNA. Samples were aliquoted and stored at −80 °C. One-hundred micrograms of protein were run on precast 4–10% polyacrylamide gels (Invitrogen). Antibodies used were to pRb Ser795 (9301), pRb Ser780 (8180), pRb Ser807 and Ser811(9308), cyclin D1 (Ccnd1) (2926), Cdk4 (2906), pErk (4370), Erk (9102), pAkt (4060), Bim (2933) (all from Cell Signaling Technologies and all used at a 1:1,000 dilution), total Rb (Abcam, ab24, 1:1,500), tubulin (Sigma, T9026, 1:4,000) and Hsp70 (BD Bioscience, 610607, 1:4,000). Samples in RIPA buffer were diluted to 1 µg µl⁻¹, and RPPA was performed by the MD Anderson RPPA Core[39].

Immunofluorescence and TUNEL staining. We performed immunofluorescence on 5 µM formalin-fixed, paraffin-embedded sections. A pressure cooker was used for antigen retrieval in 10 mM sodium citrate buffer, pH 8.5, at 110 °C for 10 min. Antibody against pH 3 (Cell Signaling Technologies, 9701) was diluted 1:300 in 1% BSA, PBS and Tween 20 (PBST) and incubated overnight at 4 °C. Biotinylated secondary antibody (Abcam) signals were amplified with streptavidin–horseradish peroxidase (Biogenex), fluorescence was developed using a tetramethylrhodamine Tyramide TSA-Plus kit (PerkinElmer), and slides were counterstained with DAPI. TUNEL staining was performed using the Apoptotag Red kit (Millipore) as per the manufacturer's instructions. Positive signals were counted on a fluorescent microscope using DAPI and adjacent H&E sections to discriminate between tumor and nontumor regions. All signals were counted per tumor. Fluorescence images were taken using a CoolSnap ES2 camera (Photometrics) and NIS-Elements software (Nikon). Brightness levels were slightly and uniformly elevated within and across all samples, but the pictures were otherwise unprocessed. H&E sections were photographed on a light microscope, and Adobe Photoshop was used to measure the tumor area.

Cell culture. We isolated iNRAS melanoma cell lines from primary tumors by collagenase digestion followed by culture in RPMI and 10% FBS supplemented with 2 mg ml⁻¹ doxycycline (Research Products International). Eleven iNRAS cell lines were assayed for tumor development and doxycycline dependence in nude mice. iNRAS lines 413 and 475 were selected for efficient tumor formation, regression after doxycycline withdrawal and complete loss of transgene expression by quantitative RT-PCR. Both cell lines were always used as low-passage (less than eight) cultures, maintained in RPMI and 10% FBS supplemented with 2 mg ml⁻¹ doxycycline. HMVII is a mycoplasma-free human melanoma cell line,

which was maintained in RPMI and 10% FBS. SB-2 was maintained in Eagle's Minimal Essential Medium (EMEM) (AATC) and 10% FBS.

Animal studies. iNRAS mice harbor three genetically engineered alleles: a constitutive *Cdkn2a* knockout[40], a new tetO-*NRAS*[Q61K] transgene and a Tyr-rtTA transgene[20]. TetO is a multimerized tet operon that drives *NRAS*[Q61K] expression only in the presence of both rtTA and doxycycline. All mice had been backcrossed for at least eight generations onto the FVB/N strain. Mice intended for tumor development are weaned onto 2 mg ml⁻¹ doxycycline (Research Products International) in drinking water containing 5% sucrose (Sigma) at 3–4 weeks of age.

All xenograft studies used female immunodeficient nude mice (Taconic). One million cells in HBSS (Gibco) were injected intradermally into the flank. Tumor volumes were calculated using electronic calipers to measure the length (l), width (w) and height (h) and using the formula (l × w × h) × π/6. Body mass was measured using an electronic scale.

We dissolved selumetinib or GSK1120212 in sterile 100% DMSO and diluted it 1:9 in sterile-filtered 1% carboxymethylcellulose and 0.4% Tween-80 (Sigma). We dissolved PD-0332991 directly in sterile filtered 50 mM sodium lactate, pH 4.0 (Sigma). Oral gavage was delivered using sterile flexible plastic adapters in 100 µl or 200 µl doses when tumors reached between 100 mm³ and 200 mm³ in volume. Because MEKi and inhibitors of CDK4/6 (CDK4/6i) are formulated at different pHs, mice on the inhibitor combination were fed with a minimum of 4 h in between doses of MEKi and CDK4/6i. MEKi was always fed first if the inhibitors were given on the same day. Within each experiment, mice received MEKi or CDK4/6i at the same time across cohorts.

We measured BrdU incorporation rates *in vivo* by injecting mice intraperitoneally with 1 mg of BrdU in PBS (BD Biosciences) 24 h before they were euthanized and concomitant with the second-to-last dose of GSK1120212 or vehicle. The final dose of GSK1120212 or vehicle was administered 8 h before euthanasia. All animal experiments were performed according to protocols approved by the Institutional Animal Care and Use Committees at the Dana-Farber Cancer Institute and the University of Texas MD Anderson Cancer Center.

Patient sample. A 47-year-old female patient with metastatic melanoma containing an NRAS mutation (confirmed by genotyping to contain the mutation Q61K) was consented for tissue acquisition per Institutional Review Board (Massachusettes General Hostpital, Partners Human Research Committee)–approved protocol. A tumor biopsy was performed, and portions of the resected tumor were harvested and processed for EVOC (see below). Additional tissue was formalin fixed and analyzed to confirm that viable tumor was present by H&E staining. Tissue was also snap frozen and stored at −80 °C or was immediately processed for purification of RNA and DNA.

Clinical data regarding the patient sample. The 47-year-old female patient mentioned above was diagnosed with a thin melanoma of the left lower extremity in 2007 and underwent wide local excision. She developed a mass in the surgical scar in 2009 and underwent re-excision of the area with sentinel node mapping and biopsy (two of three nodes were positive for metastatic melanoma). She then underwent completion lymphadenectomy and received adjuvant interferon (which was discontinued because of side effects). In 2011, she developed multiple metastatic lesions in the left lower extremity and was treated with interleukin-2 and progressed on therapy. She then was treated on a clinical trial with combined anti–cytotoxic T lymphocyte antigen 4 (CTLA-4) blockade and vascular endothelial growth factor (VEGF) inhibitor and progressed on therapy with an increase in the size of existing lesions and new lesions in other sites (adrenal, lung and subcutaneous). She underwent genotyping of her tumor, which showed no BRAF mutation but did show an NRAS mutation. She presented for a discussion for options of further therapy with investigational agents and was consented on tissue protocol as described previously. This was approved by the Dana-Farber Cancer Institute Institutional Review Board on 22 August 2011 (DFCI Legacy #11-181, Assurance #FWA00001121).

EVOC. We performed the EVOC as described in Vaira *et al.*[41]. In brief, freshly resected tumor tissue was sectioned at 300-µm thickness using a vibratome. These slices were cultured in DMEM/F10 Ham's media plus 10% FBS on top

of Millicell cell-culture inserts (Millipore) for 72 h with DMSO or inhibitors. Twenty-four hours before harvest, cultures were re-fed with media containing BrdU (Invitrogen, 93-3943). After harvest, tissue was subject to routine tissue processing. Five-micron paraffin sections were stained for BrdU (Invitrogen), cleaved caspase-3 (9664, Cell Signaling) and pErk (4376, Cell Signaling). Slides were digitally scanned using the Aperio ScanScope XT slide scanning system, and seven to nine bounded areas of representative staining were identified for quantification with Aperio ImageScope software. Representative regions of tumor sections were selected based on histological appearance. Individual regions were counted for positive cells, and the sum was divided by the total area, as quantified using histomorphometric analysis tools in ImageScope.

Identification of the NRAS-MAPK gene set. We filtered our mouse melanoma NRAS extinction and MEKi microarray datasets by comparison to publicly available datasets. These sets measured BRAF-mutant human melanoma cell lines and xenografts treated with MEK inhibitors, BRAF inhibitors or inducible BRAF shRNAs. These sets were retrieved from ArrayExpress (http://www.ebi.ac.uk/arrayexpress/) or the Gene Expression Omnibus (http://www.ncbi.nlm.nih.gov/geo/) with the designations E-GEOD-2005 (ref. 31), E-GEOD-13487 (ref. 33), GSE17089 (ref. 32) and E-GEOD-35230. We set criteria of a significant change in both of our mouse datasets ($Q < 10^{-3}$) and a significant change in at least three of the four human datasets (Student's t test comparing treated to control samples, $P < 0.05$). Forty-nine genes met these criteria. A knowledge-based assessment of the gene set identified a strong enrichment for known ERK targets and sensors such as MAFF, FOSL1, ETV1, ETV4, ETV5, DUSP4 and DUSP6 (**Supplementary Table 8**).

Taking the average of the gene set is one way to compare across samples. However, not all 49 genes behaved proportionally to each other from sample to sample, which is probably a result of differing kinetic profiles for each gene and condition. Therefore, in addition to the average, we wanted to generate a gene-set–wide statistic that could compare samples despite these inter-gene fluctuations. A paired, two-tailed Student's t test restricts the comparisons between matched gene measurements while calculating the significance of the entire set.

Identification and prioritization of RSM genes and proteins. We first compared transcript expression values as measured on Affymetrix MG403_2 microarrays for doxycycline withdrawal to vehicle and selumetinib treatment to vehicle. The statistical significance for each comparison was determined using linear models in the R package limma[42], and P values were corrected using the Benjamini-Hochberg method. Additionally, log-transformed ratios were calculated for each comparison. The graph in **Figure 1b** plots the $\log_2$ fold change values for doxycycline withdrawal compared to selumetinib treatment. Genes that lie near the regression line are genes that are changed in the same direction by both treatments and to a relatively similar magnitude.

To select genes that showed differential expression under the different treatments, we sought to identify and rank genes that lie away from the regression line. To do so, we applied a modified version of Fisher's method to combine P values as a way to introduce a statistical penalty for genes that change in the same direction and reward genes that change in opposite directions. We use r to represent the P value of a gene under doxycycline withdrawal and m to represent the P value of a gene under selumetinib treatment.

If the gene changes in opposite directions, then:

$$\chi^2 = -2(\ln(r) + \ln(m))$$

If the gene changes in the same direction and $r < m$, then:

$$\chi^2 = -2(\ln(r) - \ln(m))$$

If the gene changes in the same direction and $m < r$, then:

$$\chi^2 = -2(\ln(m) - \ln(r))$$

The resulting ranked gene list prioritizes genes that change in opposite directions for the two treatments and also those that are significantly changed by one treatment but not the other. This prevents a bias regarding whether there is a unidirectional gradient for all MAPK signaling targets and can also uncover any off-target effects of selumetinib. We refer to this ranked list as the RSM.

The same statistical procedure was applied to the reverse-phase protein array data to identify RSM proteins.

Identification and prioritization of RSM pathways. The top 864 genes from the RSM-ranked gene list ($P < 10^{-5}$) were selected for processing through Metacore (Geneco, Inc.) software available online using default settings. Ranked pathways were generated using the 'analyze single experiment' feature with default settings. The top ten results of these analyses are presented in **Supplementary Table 4**.

GSEA was performed on the entire list of 19,623 RSM-ranked genes. Genes were assigned a direction of change (doxycycline withdrawal compared to selumetinib treatment) to complement the statistical measure calculated by the modified Fisher's method described above. Full results of these analyses are supplied in **Supplementary Table 3**.

Hierarchical clustering. Hierarchical clustering was performed using the MultiExperiment Viewer software (http://www.tm4.org/mev/).

Construction of the TRAP network. The TRAP network aims to identify regulatory relationships between known transcriptional regulators and putative biological pathways. The construction of the TRAP network can be broken into four separate components, and the detailed methods and materials for each step are as follows: (i) identification of known transcriptional regulators, (ii) building gene sets that are defined by annotated biological pathways (for example, Wnt signaling, ribosome biogenesis, purine metabolism, and so on), (iii) compiling a compendium of microarray data and computing the putative expression of pathways and (iv) computing a measure of statistical significance between all regulators and pathways using mutual information.

Defining transcriptional regulators. A mouse gene was defined as a 'regulator' if it met any of the following criteria: the gene was annotated with the following terms from the Gene Ontology (http://www.geneontology.org/): GO:0006351 (transcription- and DNA-dependent) or GO:0008134 (transcription-factor binding). Annotations with evidence codes of IEA, ND and NR were excluded. A gene was defined as a transcription factor by the DBD: Transcription Factor Prediction Database (http://www.transcriptionfactor.org/). A gene was annotated as a transcription factor by the Riken Transcription Factor Database (TFdb) (http://genome.gsc.riken.jp/TFdb/).

Constructing pathway gene sets. We use the terms 'biological pathway' or simply 'pathway' to describe a set of genes that function together to perform a specific biological process. We start off with the set of pathways defined under the 'C2:canonical pathways' collection from the MSigDB. Under version 3.0 of MSigDB, there are 880 sets of genes that are annotated as canonical pathways. Within this set, there are many pathways that have a high degree of overlap. In an effort to compile pathways that are as independent as possible (in other words, reduce the overlap in genes shared between pathways), we required that a pathway have a maximum overlap of 80% as defined by the Jaccard distance,

$$J(A, B) = \frac{|A \cap B|}{|A \cup B|}$$, where A represents the gene list for pathway A and B

represents the gene list for pathway B. After filtering, the final list of canonical pathways was reduced to 431.

The expression of pathway, p_i, is calculated as the average expression of the

constituent genes of p_i, $p_i = \frac{1}{n}\sum_{j=1}^{n} g_j$, where $p_i = \langle g_1, g_2, \ldots, g_n \rangle$ and g_j is

the log-transformed expression value for gene j.

Compiling a microarray compendium. Over 10,000 individual microarrays across a range of experimental conditions were downloaded from the publicly available microarray repositories ArrayExpress and Gene Expression Omnibus (GEO) (http://www.ncbi.nlm.nih.gov/geo/). All files were raw data (.CEL files) and were selected from the same Affymetrix platform, Mouse Genome 430 2.0. The entire compendium was normalized together using the robust multiarray averaging (RMA) method of background subtraction, quantile normalization, and summarized using median polish[43]. This resulted in a probeset-by-condition

matrix of log-transformed expression values. Probesets were mapped to gene symbols using the Affymetrix library files, and multiple probesets mapping to one gene were averaged.

The large number of arrays is intended to cover the widest range of experimental perturbations possible, though there was a great degree of overlap between arrays. That is, there were many arrays that showed correlation of transcript expression with $r^2 > 0.98$. To reduce the oversampling of very similar expression profiles, we removed, in a pairwise manner, one array at random in the pair if the correlation was measured at $r^2 > 0.95$. The final filtered compendium consisted of 3,103 microarrays.

Connecting regulators to pathways through mutual information. The details of the statistical method we used to connect regulators to pathways drew heavily from the context likelihood of relatedness (CLR) method[44]. The simple modification we used here was to treat regulator gene expression and putative pathway expression as the input, whereas CLR takes gene expression from individual genes as the input.

The TRAP algorithm is shown in **Supplementary Figure 6** and proceeds in two phases. First, a mutual information matrix, *M*, is calculated between all pairwise regulators and pathways. Mutual information is calculated as:

$$I(X;Y) = \sum_{i,j} P(x_i, y_j) \frac{P(x_i, y_j)}{P(x_i) \times P(y_j)}$$

where *X* represents the vector of expression values for the regulator or pathway *i*, and *Y* represents the vector of expression values for the regulator or pathway *j*.

The second phase of the TRAP algorithm is to calculate the likelihood that a regulator is connected to a pathway. As shown in **Supplementary Figure 6**, within *M*, there is a set of cells where the regulators are the rows and the pathways are the columns (red) and another group of cells where the pathways are the rows and the regulators are the columns (blue). Within these two groups,

column *j* is z-score transformed, $z_{i,j} = \frac{x_i - \mu}{\sigma}$, where μ is the column mean,

σ is the column s.d., and x_i is the expression value in row *i*. This produces two matrices, one representing the significance of the relationship between regulator *i* and pathway *j* compared to all possible pathways, and the second representing the significance between *i* and *j* compared to all possible regulators. Finally, these two z-scores are combined into a modified z score using Stouffer's method,

$$S(z_{i,j}, z_{j,i}) = \frac{z_{i,j} + z_{j,i}}{\sqrt{2}}$$

False discovery rates were estimated for the distribution of the modified z scores. For the TRAP network, we set a threshold of false discovery rate $<10^{-4}$, which corresponds to a network of 514 regulators, 391 pathways and 3,048 edges drawn between the regulators and pathways.

Selecting and ranking transcriptional regulators of cell-cycle pathways. There were 41 downregulated pathways heavily enriched for cell-cycle processes that were identified in the RSM-ranked gene list using GSEA. These 41 pathways were mapped onto the TRAP network. Next, the first-neighbor nodes from the network were selected. As the TRAP network represents regulator-to-pathway connections, the first neighbor nodes represent predicted regulators of the 41 cell-cycle–related pathways. In total, 55 neighbor regulators were selected, creating a cell-cycle–specific TRAP subnetwork (**Supplementary Fig. 6**).

The 55 regulators were then ranked on the basis of the number and strength of edges shared with the 41 cell-cycle pathways (**Supplementary Tables 7** and **8**). The strength of an edge was derived from the TRAP methodology, whereas the number of edges was determined by the count of significant pathways from the RSM-ranked gene list. These two pieces of information can be taken together to calculate a weighted degree centrality for a given regulator, where degree centrality is simply defined as the number of edges connected to a given node. We used a modified version of the weighted degree centrality measure defined in Opsahl, *et al.*[45]:

$$S_i = k_i \times \left(\frac{s_i}{k_i} \right)^{\alpha} \times \left(\frac{1}{n} \right) = k_i^{(1-\alpha)} \times s_i^{\alpha} \times \left(\frac{1}{n} \right)$$

In this equation, k_i is defined as the number of edges connected to regulator *i*, s_i is defined as the summation of the weighted edges connected to regulator *i*, and α is a tuning parameter that allows for increasing or decreasing the effect of the edge weights. For this application, we took the weights as assigned in the TRAP network and set $\alpha = 1$. The calculated weighted degree centrality was then corrected for the maximum number of edges regulator *i* can have in the network, *n*. In this instance, we selected 41 pathways in the construction of the cell-cycle–specific TRAP subnetwork, and, thus, the maximum number of edges was $n = 41$.

For comparison, we performed the same calculation of weighted degree centrality on the same 55 regulators but in the full TRAP network. By comparing the values from the cell-cycle–specific TRAP subnetwork and the full TRAP network, we are able to evaluate the relative importance of each regulator in the cell-cycle–specific TRAP network. For regulator *i*, if S_i increases in value from the full TRAP network to the cell-cycle–specific subnetwork, then regulator *i* is said to gain centrality in the network, meaning regulator *i* has a greater proportion of edges in the subnetwork as compared to in the full TRAP network. Here we aimed to identify the transcriptional regulators that are most likely to have a direct affect on the 41 significantly downregulated RSM pathways, which is reflected in the gain in the measure of weighted degree centrality. Finally, we ranked all regulators on their value of gain in centrality from the full TRAP network to the cell-cycle–specific TRAP subnetwork.

39. Paweletz, C.P. *et al.* Reverse phase protein microarrays which capture disease progression show activation of pro-survival pathways at the cancer invasion front. *Oncogene* **20**, 1981–1989 (2001).
40. Serrano, M. *et al.* Role of the INK4a locus in tumor suppression and cell mortality. *Cell* **85**, 27–37 (1996).
41. Vaira, V. *et al.* Preclinical model of organotypic culture for pharmacodynamic profiling of human tumors. *Proc. Natl. Acad. Sci. USA* **107**, 8352–8356 (2010).
42. Smyth, G.K. Linear models and empirical bayes methods for assessing differential expression in microarray experiments. *Stat. Appl. Genet. Mol. Biol.* **3**, Article3 (2004).
43. Irizarry, R.A. *et al.* Exploration, normalization, and summaries of high density oligonucleotide array probe level data. *Biostatistics* **4**, 249–264 (2003).
44. Faith, J.J. *et al.* Large-scale mapping and validation of *Escherichia coli* transcriptional regulation from a compendium of expression profiles. *PLoS Biol.* **5**, e8 (2007).
45. Opsahl, T., Agneessens, F. & Skvoretz, J. Node centrality in weighted networks: Generalizing degree and shortest paths. *Soc. Networks* **32**, 245–251 (2010).